FULL TITLE: Mayaro Virus Infection Elicits an Innate Immune Response and Represses Autophagy in *Anopheles stephensi*

SHORT TITLE: Mayaro virus infection response in an *Anopheles* model

Cory A. Henderson[1], Marco Brustolin[1], Shivanand Hegde[2], Grant L. Hughes[2], and Jason L. Rasgon[1*]

[1]Departments of Entomology and Disease Epidemiology, The Pennsylvania State University, University Park, PA, United States of America.

[2] Departments of Vector Biology and Tropical Disease Biology, Centre for Neglected Tropical Disease, Liverpool School of Tropical Medicine, Liverpool, United Kingdom

*Corresponding author: Jason L. Rasgon (jlr54@psu.edu)

Keywords: Toll Pathway, Autophagy, Transcriptome, Small RNA, miRNA, piRNA, *Alphavirus*, Mayaro Virus, *Anopheles stephensi*

ABSTRACT:

Mayaro virus (MAYV) is an arboviral pathogen in the genus *Alphavirus* that is circulating in South America with potential to spread to naïve regions. MAYV is also one of the few viruses with the ability to be transmitted by mosquitoes in the genus *Anopheles*, as well as the typical arboviral transmitting mosquitoes in the genera *Aedes and Haemagogus*. Few studies have investigated the infection response of *Anopheles* mosquitoes. In this study we detail the transcriptomic and small RNA responses of *An. stephensi* to infection with MAYV via infectious bloodmeal at 2, 7, and 14 days post infection (dpi). 361 unique transcripts were significantly regulated and 79 novel miRNAs were identified. Gene ontology analysis of transcripts regulated at each timepoint suggested activation of the Toll pathway at 2 and 7 dpi and repression of pathways related to autophagy at 14 dpi. These findings provide a basic understanding of the infection response of *An. stephensi* to MAYV and help to identify host factors which might be useful to target to inhibit viral replication in *Anopheles* mosquitoes.

AUTHOR SUMMARY:

Mayaro virus (MAYV) is a mosquito-borne Alphavirus responsible for outbreaks in South America and the Caribbean. In this study we infected *Anopheles stephensi* with MAYV and sequenced mRNA and small RNA to understand how MAYV infection impacts gene transcription and the expression of small RNAs in the mosquito vector. Genes involved with innate immunity and autophagy are regulated in response to MAYV infection of *An. stephensi.* We also discovered novel miRNAs and described their expression patterns following bloodmeal ingestion. These results suggest that MAYV does induce a molecular response to infection in its

mosquito vector species and that MAYV may have mechanisms to evade the vector immune response.

INTRODUCTION

Mayaro virus (MAYV) is a mosquito-borne, enveloped positive-sense single-stranded RNA virus in the genus *Alphavirus*, first isolated from the blood of five febrile workers in Mayaro county, Trinidad in 1954 [1]. Symptoms of MAYV infection are similar to other arboviral infections such as dengue or Chikungunya viruses, and include rash, fever, retro-orbital pain, headache, diarrhea, and arthralgia [2]. While no epidemics or outbreaks with Mayaro virus being the causative agent have been recorded outside of South America, there have been imported cases reported in the Netherlands, Germany, France, and Switzerland [3-6], which demonstrates a need to understand the capacity for the virus to spread into naïve regions, such as the United States.

The principal mosquitoes transmitting Mayaro virus naturally are thought to be the canopy-dwellers of the genus *Haemogogus*, maintaining the sylvatic cycle between non-human primates as primary hosts and birds as secondary hosts [7]. Human infections are sporadic due to the rare display of anthropophilic biting behaviors by *Haemogogus* mosquitoes, with transmission due to these species primarily occurring in rural regions with close proximity to forests [8]. Vector competence studies have identified anthropophilic and urban adapted species such as *Aedes aegypti* and *Ae*. *albopictus,* as well as the malaria parasite transmitters *Anopheles gambiae*, *An. stephensi*, *An*. *freeborni*, and *An*. *quadrimaculatus*, as being competent vectors for Mayaro virus under laboratory conditions [9-12]. Transmission of an arbovirus with an anopheline mosquito as a primary vector is rare, only having been observed occurring regularly for O'nyong'nyong virus by *An. gambiae* and *An. funestus* in Uganda [13], with some limited evidence for Chikungunya and Semliki Forest virus [14]. As arboviral pathogens are transmitted between hosts primarily by arthropod vectors, transmission requires the virus to

infect and disseminate from the midgut and salivary glands of the mosquito following an infectious bloodmeal [15]. The molecular underpinnings controlling why MAYV and these closely related viruses can infect and be transmitted by *Anopheles* mosquitoes is of epidemiological interest, yet remains poorly understood. A more complete understanding of this phenomenon requires investigation of the molecular pathways involved in viral infection of anopheline mosquitoes. Recent transcriptomic studies have identified a number of genes involved in classical immune pathways, RNA interference (RNAi), metabolism, energy production, and transport as being regulated in response to arboviral infection of mosquitoes [16-19]. In addition, studies focusing on small RNA identification and regulation have identified RNAi activity, such as miRNA and piRNA expression, in response to infection of mosquitoes by arboviruses [20-23].

The available evidence suggests that, should MAYV be introduced into a naïve region, outbreaks and epidemics of the resulting disease could be driven by anopheline vectors [9, 24-25]. Because anopheline, and not aedine, mosquitoes could act as the primary transmitting vectors for MAYV, this study also provides an opportunity to understand how vector competence might emerge in this system and provide insight into why *Anopheles* are generally poor viral transmitters when compared to *Aedes* mosquitoes. We used RNA sequencing to study the transcriptomic and small RNA responses of *An. stephensi* to infection with MAYV via infectious bloodmeal at 2, 7, and 14 days post infection (dpi).

MATERIALS AND METHODS

Anopheles stephensi Rearing

Protocols pertaining to mosquito rearing and presentation of infectious bloodmeal has been described elsewhere [9]. Briefly, *An. stephensi* (Liston strain) were provided by Johns Hopkins University (Baltimore, MD, USA). Mosquito colonies were reared and maintained at the Millennium Sciences Complex insectary (The Pennsylvania State University, University Park, PA, USA) at 27˚C ± 1˚C, 12 hour light 12 hour dark diurnal cycle at 80% relative humidity in 30×30×30-cm cages. Ground fish flakes (TetraMin, Melle, Germany) were used to feed larvae, and upon emergence adult mosquitoes were maintained with a 10% sucrose solution.

Viral Production and Infection via Bloodmeal

Mayaro virus strain BeAn 343102 (BEI Resources, Manassas, VA, USA) was utilized in this study, a genotype D strain originally isolated from a monkey in Para, Brazil, in May 1978. Virus-infected supernatant was aliquoted and stored at −80˚C until used for mosquito infections. Viral stock titers were obtained by focus forming assay (FFA) technique. Adult female mosquitoes at 6 days post emergence that had not previously blood-fed were used for experimentation. Mosquitoes were allowed to feed on either human blood spiked with Mayaro virus at 1*107 FFU/mL or a control bloodmeal with no virus via a glass feeder jacketed with 37˚C distilled water for 1 h.

At 2, 7, and 14 days post infection, mosquitoes were anesthetized with triethylamine (Sigma, St. Louis, MO, USA) and RNA was extracted from each individual mosquito using mirVana RNA extraction kit (Life Technologies) applying the protocol for extraction of total RNA. Infection was confirmed via qPCR using primers published by Wiggins et. al. 2018 (Forward: 5′-TGGACCTTTGGCTCTTCTTATC-3′, Reverse: 5′-GACGCTCACTGCGACTAAA-3′) [10], a CT value of 20 or less was used to confirm infection (Supplementary Table 1). 3 pools of total RNA were created for each time point and infection status to be used for library preparation, each

consisting of 750 ng of RNA from 4 mosquitoes for a total of 3 mg per pool as confirmed via Nanodrop. The protocol for mosquito rearing, viral production, and infection via bloodmeal is described in more detail in Brustolin et al. 2018 [9].

Transcriptomic Library Preparation and Sequencing

All pools were sent to University of Texas Medical Branch for library preparation where total RNA was quantified using a Qubit fluorescent assay (Thermo Scientific) and RNA quality was assessed using an RNA 6000 chip on an Agilent 2100 Bioanalyzer (Agilent Technologies). See Etebari et all. 2017 for more detail on library preparation and sequencing [17]. 1 mg of total RNA per pool was poly-A selected and fragmented using divalent cations and heat (940 C, 8 min). The NEBNext Ultra II RNA library kit (New England Biolabs) was used for RNA-Seq library construction. Fragmented poly-A RNA samples were converted to cDNA by random primed synthesis using ProtoScript II reverse transcriptase (New England Biolabs). After second strand synthesis, the double-stranded DNAs were treated with T4 DNA polymerase, 5' phosphorylated and then an adenine residue was added to the 3' ends of the DNA. Adapters were then ligated to the ends of these target template DNAs. After ligation, the template DNAs were amplified (5-9 cycles) using primers specific to each of the non-complimentary sequences in the adapters. This created a library of DNA templates that have non-homologous 5' and 3' ends. A qPCR analysis was performed to determine the template concentration of each library. Reference standards cloned from a HeLa S3 RNA-Seq library were used in the qPCR analysis. Cluster formation was performed using 15.5-17 billion templates per lane using the Illumina cBot v3 system. Sequencing by synthesis, paired end 75 base reads, was performed on an Illumina NextSeq 5500 using a protocol recommended by the manufacturer.

Small RNA Library Preparation and Sequencing

Small RNA libraries were created using the New England Biolabs small RNA library protocol. See Saldaña et. al. 2017 for more information on small RNA sequencing [21]. Library construction used a two-step ligation process to create templates compatible with Illumina based next generation sequence (NGS) analysis. Where appropriate, RNA samples were quantified using a Qubit fluorometric assay. RNA quality was assessed using a pico-RNA chip on an Agilent 2100 Bioanalyzer. Library creation uses a sequential addition of first a 3' adapter sequence followed by a 5' adapter sequence. A cDNA copy was then synthesized using ProtoScript reverse transcriptase and a primer complimentary to a segment of the 3' adapter. Amplification of the template population was performed in 15 cycles (94˚C for 30 sec; 62˚C for 30 sec; 70˚C for 30 sec) and the amplified templates were PAGE (polyacrylamide gel electrophoresis) purified (147 bp DNA) prior to sequencing. All NGS libraries were indexed. The final concentration of all NGS libraries was determined using a Qubit fluorometric assay and the DNA fragment size of each library was assessed using a DNA 1000 high sensitivity chip and an Agilent 2100 Bioanalyzer. Single end 75 base sequencing by synthesis on an Illumina NextSeq 5500.

Transcriptomic RNA Sequencing Data Analysis

Raw sequencing data was uploaded to the ICS-ACI high performance computing cluster at Pennsylvania State University to perform all computational analyses. Transcriptomic libraries had adapters were trimmed and low-quality bases removed using Trimmomatic read trimming software with base settings [26]. Quality trimmed reads were aligned to the current build of the Anopheles stephensi Indian strain genome in Vectorbase (AsteI2) using the STAR RNA sequencing aligner [27]. Reads less than 75 bp in length and with a mapping quality of less than 20 were dropped from the analysis, and read counts were calculated in R using the rSubread

package [28], following which a principal components analysis was performed and differential expression conducted using a negative binomial GLM with the EdgeR package [29]. Contrasts considered in the GLM were infected against control at 2, 7, and 14 dpi, and differences between 2 -7 dpi and 7 – 14 dpi for infected and control treatments. Gene IDs that were differentially expressed with a LogFC value of +/- 1 and FDR < 0.05 were uploaded to g:Profiler to run GO term overrepresentation analysis [30].

Small RNA Sequencing Data Analysis

Small RNA libraries had adapters trimmed using Trimmomatic and were subsequently passed into the miRDeep2 pipeline to identify novel and known miRNAs in all samples and determine expression of all known and novel miRNAs at each time point and treatment status [31, 26]. Novel miRNAs with a miRDeep score of less than 3, a minimum free energy value of less than – 20, or a non-significant Randfold p-value were considered false IDs and excluded from further analysis. miRNA targets were identified in the AsteI2 genome using miRanda software package [32]. Differential expression of miRNAs in response to infection status and time point was conducted using a negative binomial GLM with the EdgeR package and contrasts as described for the transcriptomic analysis [29]. miRNAs which were differentially expressed with LogFC +/- 1 and FDR < 0.05 had their miRanda genomic targets uploaded to g:Profiler to determine if any GO terms were overrepresented by transcripts potentially regulated by differentially expressed miRNAs [36]. piRNAs were isolated from the small RNA libraries by selecting all 24 – 30 nt reads from the trimmed datasets and filtering out all identified mature miRNAs, and those mapping to the AsteI2 genome were considered potential piRNAs. piRNA alignment to the AsteI2 genome was performed using STAR RNA sequencing aligner allowing for 3 mismatches across the length of the read [27].

RESULTS/DISCUSSION

Transcriptome

RNA Sequencing

We assayed genome-wide gene expression in pools of *An. stephensi* (Liston strain) individuals experimentally infected with MAYV at 2, 7, and 14 dpi, along with blood fed uninfected negative controls. RNAseq libraries were sequenced on the Illumina NextSeq 5500 platform, yielding 20.6 - 28.4 million paired end reads per library. (Supplementary Table 1). Principal components analysis (PCA) performed on read counts of each annotated gene in the *An. stephensi* (Indian strain) reference transcriptome (AsteI2) at each time point distributed infected and control samples into distinct groups (Figure 1).

Differential Expression

To determine which genes exhibit differential expression by infection status and between time points a general-linearized model (GLM) was performed on filtered and normalized read counts mapping to the AsteI2 genome (Table 1, details in Supplementary Table 2; Figure 2; Figure 3). Contrasts considered in the GLM were infected compared to control at 2, 7, and 14 dpi, and differences between 2 -7 dpi and 7 – 14 dpi for infected and control treatments. Genes were considered significantly regulated if they had a log fold-change (log2FC) value of +/= 1 and FDR < 0.05.

There were 173 (71 enriched, 101 depleted), 76 (48 enriched, 28 depleted), and 200 (146 enriched, 54 depleted) of 10,313 annotated genes regulated between control and infected at 2, 7, and 14 dpi respectively. Eight genes were regulated in the same direction at each time point, 7 enriched (ASTEI08024, ASTEI02862, ASTEI03083, ASTEI10874, ASTEI08260, ASTEI07890, ASTEI07892) and 1 depleted (ASTEI04716). The gene with the strongest response to infection at

any time point was ASTEI04601 at 2 dpi with a logFC of -9.8 and the most enriched gene was ASTEI04639 at 14 dpi with logFC pf 5.7.

When considering changes between time points for the infected treatment, there were 145 positively and 416 negatively regulated genes between 2 - 7 dpi, and 644 upregulated and 325 downregulated genes between 7 - 14 dpi. To determine the impact of infection relative to control, genes that were differentially expressed between timepoints for the control treatment were filtered from the infected treatment results if they were regulated in the same direction. After filtering the control response from the infected response, 76 of the upregulated and 62 of the downregulated genes between 2 - 7 dpi remained, and 485 upregulated and 313 downregulated genes remained between 7 - 14 dpi. There was a very strong depletion response from 2 – 7 dpi in the infected treatment with logFC values reaching -15 (ASTEI06245 and ASTEI04566). Most of the genes depleted in the infected treatment correspond with those observed in the control grouping, suggesting many of the differences between the time points are due to genes that are highly expressed post-bloodmeal and not due to infection. Of those regulated genes that were to unique to the infection treatment between 2 and 7 dpi logFC ranged from -5.8 (ASTEI08794) to 2.4 (ASTEI02857), and for 7 to 14 dpi they ranged from -3.2 (ASTEI08604) to 5.3 (ASTEI02210).

Gene Ontology

A gene ontology (GO) over-representation analysis was performed using g:Profiler on gene IDs which were significantly enriched or depleted in any considered contrast in the GLM described above, and terms were considered significant if they had an FDR < 0.05 (Supplementary Table 3) [36]. At 2 dpi no downregulated terms were considered overrepresented, but upregulated terms were biased by catalytic enzymes, specifically serine

type endopeptidases for molecular function, and proteolysis was the only biological function term overrepresented at 2 dpi. At 7 dpi there was more serine type endopeptidase activity in the enriched grouping performing proteolysis in the cellular membrane, but the most overrepresented term in the downregulated group of genes at 7 dpi wasfor odorant binding, with acyltransferases and dioxygenases also being overrepresented by downregulated genes at 7dpi. At 14 dpi the highest number of GO terms were regulated than at any other time point and this is the grouping that saw the highest diversity of terms overrepresented. Molecular functions such as transferase regulation, melanin biosynthesis, cell death, reproduction, NF-kB signaling, and MAPK/JNK signaling were overrepresented by downregulated genes at 14 dpi, with activity being localized to peroxisomes and nucleosomes, while terms upregulated at 14 dpi were only identified as being involved with perception of external stimuli.

Between 2 and 7 dpi only two terms associated with steroid biosynthesis were overrepresented in the grouping of downregulated genes which were unique to infection status. Unique genes regulated in the infection group between 7 to 14 dpi saw more overrepresentation of GO terms, with many terms associated with either binding and signaling or lipid metabolism being overrepresented by upregulated genes, and terms related to cell division, DNA repair, and MAPK/JNK cascades being represented by downregulated genes. Serine proteases were upregulated at early stages of infection with Mayaro virus, suggesting an initial activation of the Toll pathway as part of the innate humoral response to infection [33]. Activation of serine proteases is not uncommon in early stages of pathogenic infection of insects, and has been identified specifically as upregulated in *Ae. aegypti* in response to dengue and Zika virus infection, and in *An. gambiae* and *An. coluzzii* in response to O'nyong'nyong virus infection [16-18, 34]. At late stages of infection there was depletion of the autophagic inducing

JNK and MAPK cascades in addition to repression of JAK/STAT signaling pathways through repression of NF-kB and MAPK signaling, both of which have positive impacts on alphaviral replication [35 – 36]. There was also upregulation of iron binding proteins which might suggest host sequestration of iron in response to viral infection [37 – 38], as well as an upregulation of lipases which should lead to the production of lipid droplets which accumulate in immune challenged cells and aid in the recruitment of signaling molecules following Toll-like receptor activation [39].

Small RNA

miRNA Identification

We next identified novel miRNAs in the small RNA transcriptomes of the MAYV infected samples and controls using miRDeep [31]. We searched for matches in our sequencing reads to all miRNAs in the miRBase database for the species *An. gambiae*, *Aedes aegypti, Culex quinquefasciatus, Drosophila melanogaster, Bombyx mori, Apis mellifera,* and *Acyrthosiphon pisum*. We found matches to 74 known miRNAs, all from *An. gambiae*, and 79 novel miRNAs identified across all samples, with between 2.2 – 4.0 million reads mapping to identified miRNAs per-sample (Supplementary Table 4). We found no explicit relationship between diversity of miRNA population and either dpi or infection status. Of the 153 total miRNAs identified across all samples, 83 were present in at least one replicate per treatment (Figure 4). PCA of read counts for all identified miRNAs in each sample showed no obvious grouping patterns at 2 and 7 dpi, however there was a correlation between infection status and PC1/PC2 placement at 14 dpi (Figure 5).

miRNA Differential Expression

We next identified known and novel miRNAs that were differentially expressed by infection status (Fig. 6; Table 2, Supplementary Table 5). Contrasts considered in the GLM were infected against control at 2, 7, and 14 dpi, and differences between 2 -7 dpi and 7 – 14 dpi for infected and control treatments, and miRNAs were considered differentially expressed by having a log fold-change (logFC) value of +/- 1 and FDR < 0.05.

There were a total of 5 miRNAs differentially regulated in any considered contrast, 1 novel miRNA (as-mir16) was upregulated and 1 known miRNA (aga-miR-286b-5p) was downregulated at both 2 and 7 dpi in the infected treatments, and 3 additional miRNAs were also downregulated at 7 dpi but not at 2 dpi (aga-miR-2944a-5p, aga-miR-2944b-5p, and aga-miR-309). No miRNAs were regulated at 14 dpi between infected and control. as-mir16 was upregulated in the infected treatment between 2 and 7 dpi but not in the control, however it was upregulated between 7 and 14 dpi in the infected and control groups. Between 2 and 7 dpi all 4 downregulated miRNAs are identified as downregulated in infected and control treatments, but the magnitude of downregulation is much higher in the infected vs control treatments. Between 7 ad 14 dpi, aga-miR-2944b-5p and aga-miR-309 were downregulated in the infected treatments, while all 4 downregulated miRNAs were downregulated in the control treatment.

The miR-309/286/2944 has been found to be upregulated in *An. gambiae* in response to bloodfeeding [40 – 41], and to be associated with Argonaute proteins post-bloodmeal [40]. When experimentally repressed aga- miR-309 was found to retard oocyte development [40], so it's down-regulation in response to MAYV infection may suggest that viral replication sequesters resources normally requires for host oocyte development, and as a result associated miRNA are also downregulated.

<u>miRNA Target Prediction</u>

We next identified putative targets in the *An. stephensi* genome for all known and novel miRNAs identified in all samples (Table 3) [32]. For each of the identified miRNAs we found an average 537 potential annotated targets within the Astel2 genome (Supplementary Table 6). Targets for significantly regulated miRNAs were loaded into g:Profiler and any overrepresented GO terms with an FDR < 0.5 were considered significant [36].

as-mir-16 was the only identified miRNA which was significantly upregulated in response to infection, but the only GO terms overrepresented by the predicted genomic targets of this miRNA are binding and protein binding for molecular function. aga-miR-286b-5p was downregulated in all contrasts considered except at 14 dpi, but it had no GO terms overrepresented by its predicted genomic targets. aga-mir-2944a-5p and aga-mir-2944b-5p were both downregulated at 7 dpi and between 2 – 7 dpi and 7 – 14 dpi for infected and control treatments and both have GO terms primarily associated with intracellular signaling and various binding functions, and aga-mir-2944b-5p also appears to be involved with lipid localization and transport.

The novel miRNA as-mir16 has 680 predicted genomic targets, and those targets overlap with 5 upregulated and 5 downregulated genes at 2 dpi, and 7 upregulated and 4 downregulated genes in response to infection. There is a slight bias for upregulated targets of this miRNA so its enhanced presence does not appear to be significantly causing downregulation as would be expected if acting as an effector molecule for RNAi [42]. As with as-mir16, the four depleted miRNAs show no significant bias between up- and down-regulated genes being targeted by the regulated miRNAs suggesting the regulation of these miRNAs is not a direct action of the virus on the miRNA, but perhaps a result of viral regulation of a downstream pathway producing regulation of the miRNAs as a result.

piRNA Identification

Virus-derived piRNA-like small RNAs (25–30 nt), have been identified in insects and insect cells infected with Flaviviruses, Bunyaviruses and Alphaviruses. Knockdown of the piRNA pathway proteins leads to enhanced replication of arboviruses in mosquito cells, suggesting their potential antiviral properties in mosquitoes [43 – 48]. For example, knockdown of Piwi-4 in *Ae. aegypti* Aag2 cell line increased replication of Semliki-Forest virus, and silencing of Ago3 and Piwi-5 led to significantly reduced production of piRNAs against Sindbis virus [44, 47].

We identified putative piRNAs in the trimmed small RNA datasets for each sample by isolating all 24-30 nt reads, removing those that were identified positively as miRNAs, and mapping the remaining reads to the Mayaro Virus BeAr 20290 genome using the STAR sequence aligner [49 – 27]. There was no particular bias for viral piRNA abundance in infected samples over control, and the proportion of potential piRNAs mapping to the viral genome remained consistent across time points (Table 4). There was a bias for piRNAs mapping to the negative strand over the positive strand, and a hotspot in the reads mapping to the negative strand at position 6990 overlapping with nonstructural protein 4 (nsP4) and at 7915 overlapping with structural C polyprotein (C) (Figure 7, Supplementary Figure 1) [50]. There does appear to be a bias in potential piRNAs mapped to the viral genome for U in position 1, but no bias for A at position 10 was observed in this study (Figure 8, Supplementary Figure 2) [51].

Mosquito cells infected with Alphaviruses and Bunyaviruses show clear U1 and A10 ping-pong piRNA signature [44, 46, 52]. In the current study reads in the 25-30 nt range mapping to the MAYV genome have a clear U1 bias but not A10, suggesting perhaps primary piRNA production without secondary piRNA biogenesis as a result as the A10 bias is suggested to be a product of cleavage activity (Figure 8) [51]. It is also observed that there are reads in the control

groupings also matching the MAYV genome with the same hotspots being produced. What may be observed is instead a general antiviral response as the viral ORFs nsP4 and C are hotspots [53], suggesting these reads are possibly constituently circulating, or expressed following bloodmeal ingestion (Figure 7).

Conclusion

The transcriptomic profiles suggest that MAYV activates the Toll pathway at early stages of infection as an innate humoral response from the host to fight infection. The Toll pathway stays upregulated until later stages of infection, when MAYV activates autophagic processes to promote replication and the *Anopheles* host responds with sequestration of iron and deposition of lipid droplets. The small RNA profiles produced suggest a potential reliance on piRNA biogenesis as a generalized antiviral immune response, but that it was not active against MAYV in this study in the sense that a ping-pong profile of potential piRNA reads mapping to the viral genome was not observed. miRNAs were also elicited in response to infection and some overlap was observed with transcripts identified as regulated in response to infection, but not to the extent that they appear to be strongly regulating transcriptional profiles in response to infection.

Acknowledgments.

We thank the UTMB sequencing core for assistance with next generation sequencing. This work was supported by NIH grants R01AI150251, R01AI128201, R01AI116636, USDA Hatch funds (Accession #1010032; Project #PEN04608), and a grant with the Pennsylvania Department of Health using Tobacco Settlement Funds to JLR, BBSRC awards BB/T001240/1 and V011278/1, Royal Society Wolfson Fellowship RSWF\R1\180013, NIH grants R21AI138074 and R21AI129507, URKI grant 20197, and NIHR grant NIHR2000907 to GLH. CAH was supported by an NSF

graduate research fellowship program award (ID 2018258101). SH was supported the Liverpool School of Tropical Medicine Director's Catalyst Fund award. GLH is affiliated to the National Institute for Health Research Health Protection Research Unit (NIHR HPRU) in Emerging and Zoonotic Infections at University of Liverpool in partnership with Public Health England (PHE), in collaboration with Liverpool School of Tropical Medicine and the University of Oxford. GLH is based at LSTM. The views expressed are those of the author(s) and not necessarily those of the NHS, the NIHR, the Department of Health or Public Health England.

References

1. Anderson CR, Wattley GH, Ahin NW, Downs WG, Reese AA. Mayaro Virus: A New Human Disease Agent. *Am J Trop Med Hyg*. 1957;6(6):1012-1016. doi:10.4269/ajtmh.1957.6.1012
2. Esposito DLA, Fonseca BAL da. Will Mayaro virus be responsible for the next outbreak of an arthropod-borne virus in Brazil? *Brazilian J Infect Dis*. 2017;21(5):540-544. doi:10.1016/j.bjid.2017.06.002
3. Hassing R-J, Leparc-Goffart I, Blank SN, et al. Imported Mayaro virus infection in the Netherlands. *J Infect*. 2010;61(4):343-345. doi:10.1016/j.jinf.2010.06.009
4. Llagonne-Barets M, Icard V, Leparc-Goffart I, et al. A case of Mayaro virus infection imported from French Guiana. *J Clin Virol*. 2016;77:66-68. doi:10.1016/j.jcv.2016.02.013
5. Receveur MC, Grandadam M, Pistone T, Malvy D. Infection with Mayaro virus in a French traveller returning from the Amazon region, Brazil, January, 2010. *Euro Surveill*. 2010;15(18). http://www.ncbi.nlm.nih.gov/pubmed/20460093. Accessed February 24, 2019.
6. Neumayr A, Gabriel M, Fritz J, et al. Mayaro virus infection in traveler returning from

Amazon Basin, northern Peru. *Emerg Infect Dis*. 2012;18(4):695-696. doi:10.3201/eid1804.111717

7. Mota MT de O, Ribeiro MR, Vedovello D, Nogueira ML. Mayaro virus: a neglected arbovirus of the Americas. *Future Virol*. 2015;10(9):1109-1122. doi:10.2217/fvl.15.76

8. Abad-Franch F, Grimmer GH, de Paula VS, Figueiredo LTM, Braga WSM, Luz SLB. Mayaro Virus Infection in Amazonia: A Multimodel Inference Approach to Risk Factor Assessment. Weaver SC, ed. *PLoS Negl Trop Dis*. 2012;6(10):e1846. doi:10.1371/journal.pntd.0001846

9. Brustolin M, Pujhari S, Henderson CA, Rasgon JL. Anopheles mosquitoes may drive invasion and transmission of Mayaro virus across geographically diverse regions. Christofferson RC, ed. *PLoS Negl Trop Dis*. 2018;12(11):e0006895. doi:10.1371/journal.pntd.0006895

10. Wiggins K, Eastmond B, Alto BW. Transmission potential of Mayaro virus in Florida *Aedes aegypti* and *Aedes albopictus* mosquitoes. *Med Vet Entomol*. 2018;32(4):436-442. doi:10.1111/mve.12322

11. Smith GC, Francy DB. Laboratory studies of a Brazilian strain of Aedes albopictus as a potential vector of Mayaro and Oropouche viruses. *J Am Mosq Control Assoc*. 1991;7(1):89-93. http://www.ncbi.nlm.nih.gov/pubmed/1646286. Accessed February 24, 2019.

12. Tesh RB, Higgs S, Hausser NL, et al. Experimental Transmission of Mayaro Virus by Aedes aegypti. *Am J Trop Med Hyg*. 2011;85(4):750-757. doi:10.4269/ajtmh.2011.11-0359

13. Rezza G, Chen R, Weaver SC. O'nyong-nyong fever: a neglected mosquito-borne viral disease. *Pathog Glob Health*. 2017;111(6):271-275. doi:10.1080/20477724.2017.1355431

14. Yadav P, Barde P, Singh D, Mishra A, Mourya D. EXPERIMENTAL TRANSMISSION OF

CHIKUNGUNYA VIRUS BY ANOPHELES STEPHENSI MOSQUITOES. *Acta Virol*. 2003;47:45-47. http://www.elis.sk/download_file.php?product_id=8&session_id=jc2533t2t4ld65j13rlddb4r55. Accessed February 24, 2019.

15. Franz A, Kantor A, Passarelli A, Clem R. Tissue Barriers to Arbovirus Infection in Mosquitoes. *Viruses*. 2015;7(7):3741-3767. doi:10.3390/v7072795

16. Bonizzoni M, Dunn WA, Campbell CL, Olson KE, Marinotti O, James AA. Complex Modulation of the Aedes aegypti Transcriptome in Response to Dengue Virus Infection. Moreira LA, ed. *PLoS One*. 2012;7(11):e50512. doi:10.1371/journal.pone.0050512

17. Etebari K, Hegde S, Saldana MA, et al. Global transcriptome analysis of Aedes aegypti mosquitoes in response to Zika virus infection. *bioRxiv*. August 2017:179416. doi:10.1101/179416

18. Waldock J, Olson KE, Christophides GK. Anopheles gambiae Antiviral Immune Response to Systemic O'nyong-nyong Infection. Traub-Csekö YM, ed. *PLoS Negl Trop Dis*. 2012;6(3):e1565. doi:10.1371/journal.pntd.0001565

19. Sim C, Hong YS, Vanlandingham DL, et al. Modulation of Anopheles gambiae gene expression in response to o'nyong-nyong virus infection. *Insect Mol Biol*. 2005;14(5):475-481. doi:10.1111/j.1365-2583.2005.00578.x

20. Palatini U, Miesen P, Carballar-Lejarazu R, et al. Comparative genomics shows that viral integrations are abundant and express piRNAs in the arboviral vectors Aedes aegypti and Aedes albopictus. *BMC Genomics*. 2017. doi:10.1186/s12864-017-3903-3

21. Saldaña MA, Etebari K, Hart CE, et al. Zika virus alters the microRNA expression profile and elicits an RNAi response in Aedes aegypti mosquitoes. Armstrong PM, ed. *PLoS Negl Trop Dis*. 2017;11(7):e0005760. doi:10.1371/journal.pntd.0005760

22. Varjak M, Donald CL, Mottram TJ, et al. Characterization of the Zika virus induced small RNA response in Aedes aegypti cells. Olson KE, ed. *PLoS Negl Trop Dis*. 2017;11(10):e0006010. doi:10.1371/journal.pntd.0006010

23. Carissimo G, Pondeville E, McFarlane M, et al. Antiviral immunity of Anopheles gambiae is highly compartmentalized, with distinct roles for RNA interference and gut microbiota. *Proc Natl Acad Sci U S A*. 2015;112(2):E176-85. doi:10.1073/pnas.1412984112

24. Sinka ME, Rubio-Palis Y, Manguin S, et al. The dominant Anopheles vectors of human malaria in the Americas: occurrence data, distribution maps and bionomic précis. *Parasit Vectors*. 2010;3(1):72. doi:10.1186/1756-3305-3-72

25. Hay SI, Sinka ME, Okara RM, et al. Developing Global Maps of the Dominant Anopheles Vectors of Human Malaria. *PLoS Med*. 2010;7(2):e1000209. doi:10.1371/journal.pmed.1000209

26. Bolger AM, Lohse M, Usadel B. Trimmomatic: a flexible trimmer for Illumina sequence data. *Bioinformatics*. 2014;30(15):2114-2120. doi:10.1093/bioinformatics/btu170

27. Dobin A, Davis CA, Schlesinger F, et al. STAR: ultrafast universal RNA-seq aligner. *Bioinformatics*. 2013;29(1):15-21. doi:10.1093/bioinformatics/bts635

28. Liao Y, Smyth GK, Shi W. The R package Rsubread is easier, faster, cheaper and better for alignment and quantification of RNA sequencing reads. *Nucleic Acids Res*. 2019;47(8):e47-e47. doi:10.1093/nar/gkz114

29. Chen Y, Mccarthy D, Ritchie M, Robinson M, Smyth GK. *EdgeR User's Guide*.; 2008. https://www.bioconductor.org/packages/release/bioc/vignettes/edgeR/inst/doc/edgeRUsersGuide.pdf. Accessed September 24, 2018.

30. Uri Reimand J¨, Arak T, Adler P, et al. g:Profiler-a web server for functional interpretation of gene lists (2016 update). *Nucleic Acids Res*. 2016;(1). doi:10.1093/nar/gkw199

31. GitHub - rajewsky-lab/mirdeep2: Discovering known and novel miRNAs from small RNA sequencing data. https://github.com/rajewsky-lab/mirdeep2. Accessed October 8, 2019.

32. Betel D, Wilson M, Gabow A, Marks DS, Sander C. The microRNA.org resource: targets and expression. *Nucleic Acids Res*. 2008;36(Database issue):D149-53. doi:10.1093/nar/gkm995

33. Kanost MR, Jiang H. Clip-domain serine proteases as immune factors in insect hemolymph. *Curr Opin Insect Sci*. 2015;11:47-55. doi:10.1016/j.cois.2015.09.003

34. Carissimo G, Pain A, Belda E, Vernick KD. Highly focused transcriptional response of Anopheles coluzzii to O'nyong nyong arbovirus during the primary midgut infection. *BMC Genomics*. 2018;19(1):526. doi:10.1186/s12864-018-4918-0

35. Samuel GH, Adelman ZN, Myles KM. Antiviral Immunity and Virus-Mediated Antagonism in Disease Vector Mosquitoes. 2017. doi:10.1016/j.tim.2017.12.005

36. Brackney DE. Implications of autophagy on arbovirus infection of mosquitoes. *Curr Opin Insect Sci*. 2017;22:1-6. doi:10.1016/j.cois.2017.05.001

37. Zhu Y, Tong L, Nie K, et al. Host serum iron modulates dengue virus acquisition by mosquitoes. *Nat Microbiol*. 2019;4(12):2405-2415. doi:10.1038/s41564-019-0555-x

38. Parrow NL, Fleming RE, Minnick MF. Sequestration and scavenging of iron in infection. *Infect Immun*. 2013;81(10):3503-3514. doi:10.1128/IAI.00602-13

39. Barletta ABF, Alves LR, Nascimento Silva MCL, et al. Emerging role of lipid droplets in Aedes aegypti immune response against bacteria and Dengue virus. *Sci Rep*. 2016;6(1):1-13. doi:10.1038/srep19928

40. Fu X, Dimopoulos G, Zhu J. Association of microRNAs with Argonaute proteins in the malaria mosquito Anopheles gambiae after blood ingestion. *Sci Rep*. 2017;7(1). doi:10.1038/s41598-017-07013-1

41. Biryukova I, Ye T, Levashina E. Transcriptome-wide analysis of microRNA expression in the malaria mosquito Anopheles gambiae. *BMC Genomics*. 2014;15(1):557. doi:10.1186/1471-2164-15-557

42. Blair CD, Olson KE. The role of RNA interference (RNAi) in arbovirus-vector interactions. *Viruses*. 2015;7(2):820-843. doi:10.3390/v7020820

43. Scott JC, Brackney DE, Campbell CL, et al. Comparison of Dengue Virus Type 2-Specific Small RNAs from RNA Interference-Competent and –Incompetent Mosquito Cells. O'Neill SL, ed. *PLoS Negl Trop Dis*. 2010;4(10):e848. doi:10.1371/journal.pntd.0000848

44. Schnettler E, Donald CL, Human S, et al. Knockdown of piRNA pathway proteins results in enhanced semliki forest virus production in mosquito cells. *J Gen Virol*. 2013;94(PART7):1680-1689. doi:10.1099/vir.0.053850-0

45. Morazzani EM, Wiley MR, Murreddu MG, Adelman ZN, Myles KM. Production of Virus-Derived Ping-Pong-Dependent piRNA-like Small RNAs in the Mosquito Soma. Ding S-W, ed. *PLoS Pathog*. 2012;8(1):e1002470. doi:10.1371/journal.ppat.1002470

46. Vodovar N, Bronkhorst AW, van Cleef KWR, et al. Arbovirus-Derived piRNAs Exhibit a Ping-Pong Signature in Mosquito Cells. Pfeffer S, ed. *PLoS One*. 2012;7(1):e30861. doi:10.1371/journal.pone.0030861

47. Miesen P, Girardi E, Van Rij RP. Distinct sets of PIWI proteins produce arbovirus and transposon-derived piRNAs in Aedes aegypti mosquito cells. *Nucleic Acids Res*. 2015;43(13):6545-6556. doi:10.1093/nar/gkv590

48. Schnettler E, Ratinier M, Watson M, et al. RNA interference targets arbovirus replication in Culicoides cells. *J Virol*. 2013;87(5):2441-2454. doi:10.1128/JVI.02848-12\

49. Espósito DLA, da Fonseca BAL. Complete genome sequence of Mayaro virus (Togaviridae, Alphavirus) strain BeAr 20290 from Brazil. *Genome Announc*. 2015;3(6). doi:10.1128/genomeA.01372-15

50. Lavergne A, Thoisy B de, Lacoste V, et al. Mayaro virus: Complete nucleotide sequence and phylogenetic relationships with other alphaviruses. *Virus Res*. 2006;117(2):283-290. doi:10.1016/j.virusres.2005.11.006

51. Brennecke J, Aravin AA, Stark A, et al. Discrete Small RNA-Generating Loci as Master Regulators of Transposon Activity in Drosophila. *Cell*. 2007;128(6):1089-1103. doi:10.1016/j.cell.2007.01.043

52. Dietrich I, Jansen S, Fall G, et al. RNA Interference Restricts Rift Valley Fever Virus in Multiple Insect Systems. *mSphere*. 2017;2(3). doi:10.1128/msphere.00090-17

53. Auguste AJ, Liria J, Forrester NL, et al. Evolutionary and Ecological Characterization of Mayaro Virus Strains Isolated during an Outbreak, Venezuela, 2010. *Emerg Infect Dis*. 2015;21(10):1742-1750. doi:10.3201/eid2110.141660

Table legends

Table 1: Differentially expressed *Anopheles stephensi* transcripts in response to Mayaro virus infection. A. – C. demonstrate differentially expressed transcripts between control and infected treatments at 2, 7, and 14 dpi respectively. D. and E. represent differentially expressed transcripts between 2 – 7 dpi and 7 – 14 dpi for infected treatments with any transcripts regulated in the same direction in the control treatments between the same time points filtered out.

Table 2: Differentially expressed *Anopheles stephensi* miRNAs in response to Mayaro virus infection. A. and B. demonstrate differentially expressed miRNAs between control and infected treatments at 2, and 7 dpi respectively. C. and D. represent differentially expressed miRNAs between 2 – 7 dpi and 7 – 14 dpi for infected and control treatments.

Table 3: Overrepresented GO terms represented by targets of significantly regulated miRNAs

Table 4: Number and proportion of reads from each small RNA sample sequenced mapping to the host genome, mapping to miRNAs, mapping to the viral genome, and of those mapping to the viral genome that are potential piRNAs.

A.

2 dpi						
gene ID	logFC	logCPM	F	P-Value	FDR	Direction
ASTEI08168	5.528023838	3.139822864	5.387740094	0.004739079	0.018069350	POSITIVE
ASTEI09093	4.018035967	2.663939429	15.43888377	1.66E-05	0.000634650	POSITIVE
ASTEI08441	3.766580380	3.817538602	4.393275027	0.011209218	0.031490369	POSITIVE
ASTEI10616	3.516092597	5.664444288	18.31733458	5.69E-06	0.000320102	POSITIVE
ASTEI02705	3.438388011	1.528631807	9.741689640	0.000246455	0.003361698	POSITIVE
ASTEI11378	3.403331545	6.591951942	19.11893056	4.33E-06	0.000272315	POSITIVE
ASTEI04118	3.385056771	5.081329351	40.26453386	2.86E-08	6.55E-06	POSITIVE
ASTEI00531	3.240777716	6.233777494	18.28453101	5.76E-06	0.000320102	POSITIVE
ASTEI07580	2.682704305	-0.78758212	8.974100386	0.000385365	0.004308472	POSITIVE
ASTEI11168	2.521860691	-1.09135028	11.46188771	9.85E-05	0.001959565	POSITIVE
ASTEI00925	2.293568300	3.082262029	15.09056596	1.91E-05	0.000696376	POSITIVE
ASTEI07890	2.214176841	0.936166449	11.11726615	0.000117352	0.002192273	POSITIVE
ASTEI05504	2.207267099	0.124358753	3.686534707	0.021908744	0.049620683	POSITIVE
ASTEI01707	2.064263449	-0.96529525	4.451084273	0.010635285	0.030413495	POSITIVE
ASTEI07892	2.039427589	2.569257967	19.19176069	1.17E-05	0.000512846	POSITIVE
ASTEI02198	-2.02489284	2.912828408	5.568187380	0.004091288	0.016603449	NEGATIVE
ASTEI05508	-2.04382102	4.367525777	6.026649442	0.002849076	0.013362983	NEGATIVE
ASTEI09416	-2.07418195	-0.99238089	4.978352799	0.006682257	0.022365284	NEGATIVE
ASTEI04602	-2.09032170	4.852065799	29.97189368	2.20E-07	3.29E-05	NEGATIVE
ASTEI08621	-2.11790438	3.340832256	6.966618384	0.001422625	0.009000072	NEGATIVE
ASTEI00155	-2.12668538	4.776202567	10.50624331	0.000161751	0.002673041	NEGATIVE
ASTEI07835	-2.16592524	4.005797194	4.224184682	0.013096873	0.034852891	NEGATIVE
ASTEI10380	-2.17892612	0.145054009	4.737083569	0.008239084	0.025691392	NEGATIVE
ASTEI00113	-2.23604636	7.353537677	11.15544437	0.000115072	0.002153591	NEGATIVE
ASTEI02435	-2.26454202	3.628893169	9.791514592	0.000239614	0.003312201	NEGATIVE
ASTEI09659	-2.27383739	2.629727973	28.98687556	2.76E-07	3.80E-05	NEGATIVE
ASTEI07450	-2.27986817	1.657875847	8.298615084	0.000583996	0.005401047	NEGATIVE
ASTEI09280	-2.28046107	2.930470102	3.805282603	0.019503583	0.045719698	NEGATIVE
ASTEI03596	-2.28559110	4.134619337	13.45980122	3.83E-05	0.001056408	NEGATIVE
ASTEI01820	-2.29240123	6.209303126	14.79372846	2.16E-05	0.000752740	NEGATIVE
ASTEI03524	-2.34824256	1.429235652	8.539615760	0.000502218	0.005016346	NEGATIVE
ASTEI03523	-2.37904181	1.999915336	9.080281165	0.000361697	0.004165283	NEGATIVE
ASTEI06119	-2.50974136	2.958073825	7.165957071	0.001237014	0.008283175	NEGATIVE
ASTEI07635	-2.53482842	8.906289919	24.30861465	9.02E-07	9.12E-05	NEGATIVE
ASTEI03160	-2.72040227	1.183066469	13.42204245	3.89E-05	0.001070748	NEGATIVE
ASTEI08671	-2.98520195	5.701221642	14.14998677	2.83E-05	0.000886177	NEGATIVE
ASTEI00189	-3.02310908	4.208833565	15.40496481	1.69E-05	0.000636965	NEGATIVE
ASTEI00191	-3.20146179	0.249448024	8.488093044	0.000518553	0.005072407	NEGATIVE
ASTEI02121	-3.47696421	3.299845565	13.95564324	3.08E-05	0.000938829	NEGATIVE
ASTEI05732	-3.69873576	4.835644867	18.14977762	6.04E-06	0.000327632	NEGATIVE
ASTEI07193	-3.97890548	4.825294448	13.31850309	4.08E-05	0.001106761	NEGATIVE
ASTEI03159	-4.08639460	5.790375208	23.07553011	1.27E-06	0.000119393	NEGATIVE
ASTEI02616	-4.10154904	0.512762825	11.98551109	7.60E-05	0.001660708	NEGATIVE
ASTEI09342	-4.92958399	7.423031097	19.83249508	3.42E-06	0.000233667	NEGATIVE
ASTEI06683	-4.97058061	2.296329248	13.07484417	4.55E-05	0.001186993	NEGATIVE
ASTEI11252	-5.35814390	2.974151453	15.49876504	1.62E-05	0.000629367	NEGATIVE
ASTEI02390	-7.64081047	5.563151762	31.22414185	6.76E-07	7.34E-05	NEGATIVE
ASTEI04601	-9.84154580	6.973440862	37.68453504	4.54E-08	9.42E-06	NEGATIVE

B.

7 dpi						
gene ID	logFC	logCPM	F	P-Value	FDR	Direction
ASTEI09440	3.43939383	7.42205049	26.1641845	5.52E-07	6.55E-05	POSITIVE
ASTEI08024	2.63510649	5.43421893	23.9640324	9.92E-07	9.68E-05	POSITIVE
ASTEI08512	2.61278461	2.52287451	21.9172645	1.85E-05	0.00068605	POSITIVE
ASTEI07892	2.51312973	2.56925797	19.1917607	1.17E-05	0.00051285	POSITIVE
ASTEI10032	2.3529647	3.83817569	3.70614329	0.02148978	0.04895131	POSITIVE
ASTEI11215	2.32985561	10.791085	237.725165	6.24E-14	5.85E-11	POSITIVE
ASTEI00207	2.27967821	-0.6972305	4.23942119	0.01291296	0.03447022	POSITIVE
ASTEI04792	2.08030998	-0.4323404	5.81232445	0.00336742	0.0147874	POSITIVE
ASTEI08260	2.05125227	1.85904011	4.39969079	0.01114384	0.03137191	POSITIVE
ASTEI00542	-2.0298268	-0.927159	6.26941854	0.00236734	0.01213319	NEGATIVE
ASTEI04716	-2.0382952	1.62696215	13.5453354	3.69E-05	0.00104142	NEGATIVE
ASTEI11356	-2.2275323	-0.6029535	11.5060406	9.63E-05	0.00194002	NEGATIVE
ASTEI05917	-2.2365867	0.66028522	5.43946268	0.00454233	0.01760259	NEGATIVE
ASTEI07216	-2.5869938	6.43866877	30.4563624	7.86E-07	8.10E-05	NEGATIVE
ASTEI04566	-2.5901828	7.1442213	25.6615096	2.18E-06	0.00017285	NEGATIVE
ASTEI07348	-3.5688425	4.15929875	17.4930276	7.62E-06	0.00037799	NEGATIVE
ASTEI08794	-4.2990462	0.70515178	3.68230571	0.02200029	0.04978429	NEGATIVE

C.

14 dpi						
gene ID	logFC	logCPM	F	P-Value	FDR	Direction
ASTEI04639	5.756292521	-0.34780434	10.52722255	0.000598346	0.005479710	POSITIVE
ASTEI10115	4.677603533	-1.07678728	4.299310718	0.012217528	0.033266026	POSITIVE
ASTEI02210	4.139223771	1.910574313	18.01581919	6.33E-06	0.000335230	POSITIVE
ASTEI06873	3.628273691	-0.28224833	7.081253097	0.005495053	0.019806010	POSITIVE
ASTEI02862	2.898224302	1.144304415	16.10424278	1.28E-05	0.000543747	POSITIVE
ASTEI08509	2.742130899	4.369875682	25.49200613	3.70E-05	0.001041470	POSITIVE
ASTEI07892	2.741719608	2.569257967	19.19176069	1.17E-05	0.000512846	POSITIVE
ASTEI02105	2.444978756	-0.06997406	32.55875981	1.25E-07	2.05E-05	POSITIVE
ASTEI11202	2.399014583	-0.84800921	7.998202625	0.000707754	0.005938458	POSITIVE
ASTEI03994	2.293128499	1.183354209	7.021369775	0.001368696	0.008814452	POSITIVE
ASTEI03385	2.291433229	0.180269452	8.449913770	0.000531045	0.005117885	POSITIVE
ASTEI11500	2.239078195	0.907158922	5.853706774	0.003259587	0.014482060	POSITIVE
ASTEI08399	2.202714795	1.221723491	4.683872578	0.008634788	0.026453339	POSITIVE
ASTEI11170	2.189349315	0.010273658	7.071324034	0.001321494	0.008657391	POSITIVE
ASTEI04566	2.180114632	7.144221304	25.66150955	2.18E-06	0.000172852	POSITIVE
ASTEI11358	2.107836901	1.104083751	5.659170675	0.003802833	0.015934506	POSITIVE
ASTEI11252	2.095376254	2.974151451	15.49876504	1.62E-05	0.000629367	POSITIVE
ASTEI08794	2.093558185	0.705151779	3.682305706	0.022000290	0.049784286	POSITIVE
ASTEI05293	2.055550254	1.965403108	6.270801081	0.002364869	0.012130235	POSITIVE
ASTEI01707	2.050575226	-0.96529525	4.451084273	0.010635285	0.030413495	POSITIVE
ASTEI06683	2.048634801	2.296329248	13.07484417	4.55E-05	0.001186993	POSITIVE
ASTEI05504	-2.03876964	0.124358753	3.686534707	0.021908744	0.049620683	NEGATIVE
ASTEI03026	-2.24983388	4.848972048	5.832692784	0.003313849	0.014634868	NEGATIVE
ASTEI08512	-2.80595811	2.522874509	21.91726452	1.85E-05	0.000686045	NEGATIVE
ASTEI08506	-3.32440527	0.868948837	28.26932757	5.09E-06	0.000305115	NEGATIVE
ASTEI08604	-3.33998058	3.982989907	10.29355700	0.000181442	0.002847840	NEGATIVE
ASTEI03019	-4.70688186	-0.10421771	3.773744883	0.020112323	0.046815414	NEGATIVE

D.

Infected 7 - 2 dpi						
gene ID	logFC	logCPM	F	P-Value	FDR	Direction
ASTEI02857	2.437915129	-0.13088335	6.830726813	0.001567124	0.009489246	POSITIVE
ASTEI10322	2.059015071	-0.22173898	6.338850720	0.002246935	0.011755913	POSITIVE
ASTEI01756	2.042751522	4.698061757	4.824138398	0.007634742	0.024374448	POSITIVE
ASTEI01542	-2.06967995	2.191847299	6.876404174	0.001516786	0.009330160	NEGATIVE
ASTEI02705	-2.45513098	1.528631807	9.741689640	0.000246455	0.003361698	NEGATIVE
ASTEI01165	-2.94478084	0.460352076	12.36565015	6.33E-05	0.001463271	NEGATIVE
ASTEI05917	-3.09233458	0.660285219	5.439462680	0.004542329	0.017602594	NEGATIVE
ASTEI04058	-3.15082856	2.785816548	8.971104569	0.000386057	0.004308472	NEGATIVE
ASTEI08441	-3.60807570	3.817538602	4.393275027	0.011209218	0.031490369	NEGATIVE
ASTEI08168	-4.40345331	3.139822864	5.387740094	0.004739079	0.018069350	NEGATIVE
ASTEI08794	-5.83011658	0.705151779	3.682305706	0.022000290	0.049784286	NEGATIVE

E.

Infected 14 - 7 dpi						
gene ID	logFC	logCPM	F	P-Value	FDR	Direction
ASTEI02210	5.338101573	1.910574313	18.01581919	6.33E-06	0.000335230	POSITIVE
ASTEI04639	4.784710050	-0.34780434	10.52722255	0.000598346	0.005479710	POSITIVE
ASTEI04566	4.174600553	7.144221304	25.66150955	2.18E-06	0.000172852	POSITIVE
ASTEI08513	4.174473056	4.543845545	97.55137119	5.39E-10	2.14E-07	POSITIVE
ASTEI00542	3.649577407	-0.92715903	6.269418539	0.002367336	0.012133186	POSITIVE
ASTEI06873	3.628273691	-0.28224833	7.081253097	0.005495053	0.019806010	POSITIVE
ASTEI04601	3.607806483	6.973440862	37.68453504	4.54E-08	9.42E-06	POSITIVE
ASTEI02105	3.375845041	-0.06997406	32.55875981	1.25E-07	2.05E-05	POSITIVE
ASTEI07216	2.742279099	6.438668773	30.45636242	7.86E-07	8.10E-05	POSITIVE
ASTEI08509	2.742130899	4.369875682	25.49200613	3.70E-05	0.001041470	POSITIVE
ASTEI05945	2.653607730	0.415608859	14.77777768	2.18E-05	0.000752740	POSITIVE
ASTEI05812	2.446916065	5.722231298	7.276317100	0.001146081	0.007889449	POSITIVE
ASTEI06978	2.422144228	0.774445793	4.948555774	0.006855394	0.022718762	POSITIVE
ASTEI07348	2.412770206	4.159298752	17.49302759	7.62E-06	0.000377988	POSITIVE
ASTEI05589	2.349207217	-0.65825735	5.607011894	0.003965294	0.016336443	POSITIVE
ASTEI03994	2.318109382	1.183354209	7.021369775	0.001368696	0.008814452	POSITIVE
ASTEI00171	2.244140837	1.352396578	13.32872157	4.06E-05	0.001104605	POSITIVE
ASTEI06822	2.200257879	0.957217145	8.338774106	0.000569383	0.005332859	POSITIVE
ASTEI08009	2.184811781	1.098068906	10.22008964	0.000188861	0.002917917	POSITIVE
ASTEI07271	2.124545729	0.703537957	4.666857973	0.008765775	0.026735485	POSITIVE
ASTEI10115	2.108597570	-1.07678728	4.299310718	0.012217528	0.033266026	POSITIVE
ASTEI03290	2.103491129	-0.23253857	4.150966387	0.014022466	0.036625700	POSITIVE
ASTEI10400	2.017044127	3.972103126	20.71585097	2.58E-06	0.000193524	POSITIVE
ASTEI03026	-2.25247390	4.848972048	5.832692784	0.003313849	0.014634868	NEGATIVE
ASTEI08512	-2.61278460	2.522874509	21.91726452	1.85E-05	0.000686045	NEGATIVE
ASTEI08604	-3.21246524	3.982989907	10.29355700	0.000181442	0.002847840	NEGATIVE

A.

2 dpi						
miRNA ID	logFC	logCPM	F	PValue	FDR	direction
as-mir16	3.954306237	2.176637416	5.056601878	0.017041175	0.046190555	POSITIVE
aga-miR-286b-5p	-1.10843641	11.18224340	8.337214718	0.000973366	0.005276672	NEGATIVE

B.

7 dpi						
miRNA ID	logFC	logCPM	F	PValue	FDR	direction
as-mir16	6.167676502	2.176637416	5.056601878	0.017041175	0.046190555	POSITIVE
aga-miR-286b-5p	-7.21380775	11.18224340	8.337214718	0.000973366	0.005276672	NEGATIVE
aga-miR-2944a-5p	-5.69239154	12.32239234	13.16192401	9.96E-05	0.001282132	NEGATIVE
aga-miR-2944b-5p	-6.22343310	10.80568208	8.518678421	0.000879472	0.005032539	NEGATIVE
aga-miR-309	-6.58441623	10.44548924	12.13136421	0.000152412	0.001569851	NEGATIVE

C.

2-7 dpi Infected						
miRNA ID	logFC	logCPM	F	PValue	FDR	direction
as-mir16	2.21337026	2.17663742	5.05660188	0.01704118	0.04619056	POSITIVE
aga-miR-286b-5p	-8.61230542	11.18224340	8.337214718	0.000973366	0.005276672	NEGATIVE
aga-miR-2944a-5p	-7.42764429	12.32239234	13.16192401	9.96E-05	0.001282132	NEGATIVE
aga-miR-2944b-5p	-7.67534371	10.80568208	8.518678421	0.000879472	0.005032539	NEGATIVE
aga-miR-309	-8.01353992	10.44548924	12.13136421	0.000152412	0.001569851	NEGATIVE
2-7 dpi Control						
miRNA ID	logFC	logCPM	F	PValue	FDR	direction
aga-miR-286b-5p	-2.50693408	11.18224340	8.337214718	0.000973366	0.005276672	NEGATIVE
aga-miR-2944a-5p	-2.38836688	12.32239234	13.16192401	9.96E-05	0.001282132	NEGATIVE
aga-miR-2944b-5p	-2.23658690	10.80568208	8.518678421	0.000879472	0.005032539	NEGATIVE
aga-miR-309	-2.22897505	10.44548924	12.13136421	0.000152412	0.001569851	NEGATIVE

D.

7-14 dpi Infected						
miRNA ID	logFC	logCPM	F	PValue	FDR	direction
as-mir16	1.5948883	2.17663742	5.05660188	0.01704118	0.04619056	POSITIVE
aga-miR-286b-5p	-3.1721881	11.1822434	8.33721472	0.00097337	0.00527667	NEGATIVE
aga-miR-309	-1.6968401	10.4454892	12.1313642	0.00015241	0.00156985	NEGATIVE
7-14 dpi Control						
miRNA ID	logFC	logCPM	F	PValue	FDR	direction
as-mir16	7.593935954	2.176637416	5.056601878	0.017041175	0.046190555	POSITIVE
aga-miR-286b-5p	-10.2986593	11.18224340	8.337214718	0.000973366	0.005276672	NEGATIVE
aga-miR-2944a-5p	-6.11696048	12.32239234	13.16192401	9.96E-05	0.001282132	NEGATIVE
aga-miR-2944b-5p	-6.06153041	10.80568208	8.518678421	0.000879472	0.005032539	NEGATIVE
aga-miR-309	-8.37508687	10.44548924	12.13136421	0.000152412	0.001569851	NEGATIVE

A.

aga-mir-2944b-5p				
Term Name	**ID**	**FDR**	**Term Size**	**Intersection Size**
Molecular Function				
protein binding	GO:0005515	7.50E-03	1791	188
Rho guanyl-nucleotide exchange factor activity	GO:0005089	7.50E-03	27	10
phosphorus-oxygen lyase activity	GO:0016849	7.53E-03	23	9
Ras guanyl-nucleotide exchange factor activity	GO:0005088	7.59E-03	29	10
nucleoside-triphosphatase activity	GO:0017111	1.12E-02	313	45
binding	GO:0005488	1.12E-02	4675	420
histone methyltransferase activity	GO:0042054	1.12E-02	12	6
histone-lysine N-methyltransferase activity	GO:0018024	1.12E-02	12	6
hydrolase activity, acting on acid anhydrides	GO:0016817	1.17E-02	328	45
hydrolase activity, acting on acid anhydrides, in phosphorus-containing anhydrides	GO:0016818	1.17E-02	325	45
pyrophosphatase activity	GO:0016462	1.17E-02	322	45
S-adenosylmethionine-dependent methyltransferase activity	GO:0008757	1.17E-02	40	11
cyclic-nucleotide phosphodiesterase activity	GO:0004112	1.17E-02	9	5
3',5'-cyclic-nucleotide phosphodiesterase activity	GO:0004114	1.17E-02	9	5
guanyl-nucleotide exchange factor activity	GO:0005085	1.17E-02	54	13
Rho GTPase binding	GO:0017048	1.42E-02	36	10
protein-lysine N-methyltransferase activity	GO:0016279	2.18E-02	15	6
lysine N-methyltransferase activity	GO:0016278	2.18E-02	15	6
guanylate cyclase activity	GO:0004383	2.79E-02	11	5
purine nucleotide binding	GO:0017076	2.79E-02	832	92
purine ribonucleotide binding	GO:0032555	2.79E-02	830	92
lipid transporter activity	GO:0005319	3.01E-02	22	7
protein methyltransferase activity	GO:0008276	3.01E-02	22	7
ribonucleotide binding	GO:0032553	3.07E-02	838	92
purine ribonucleoside triphosphate binding	GO:0035639	3.43E-02	821	90
N-methyltransferase activity	GO:0008170	3.43E-02	23	7
calcium channel activity	GO:0005262	3.43E-02	12	5
phosphoric diester hydrolase activity	GO:0008081	4.34E-02	24	7
GTPase activity	GO:0003924	4.74E-02	108	18
nucleoside phosphate binding	GO:1901265	4.86E-02	956	101
nucleotide binding	GO:0000166	4.86E-02	956	101
Biological Process				
intracellular signal transduction	GO:0035556	3.45E-06	193	42
Rho protein signal transduction	GO:0007266	4.33E-03	29	11
Ras protein signal transduction	GO:0007265	4.33E-03	40	13
cyclic nucleotide metabolic process	GO:0009187	9.48E-03	23	9
cyclic nucleotide biosynthetic process	GO:0009190	9.48E-03	23	9
regulation of Rho protein signal transduction	GO:0035023	9.48E-03	28	10
regulation of Ras protein signal transduction	GO:0046578	1.10E-02	35	11
signal transduction	GO:0007165	1.10E-02	681	84
small GTPase mediated signal transduction	GO:0007264	1.30E-02	75	17
regulation of intracellular signal transduction	GO:1902531	1.36E-02	62	15
cell communication	GO:0007154	1.59E-02	696	84
signaling	GO:0023052	1.61E-02	698	84
regulation of response to stimulus	GO:0048583	1.82E-02	94	19
response to stimulus	GO:0050896	2.51E-02	878	100
regulation of signal transduction	GO:0009966	2.64E-02	90	18
regulation of cell communication	GO:0010646	3.11E-02	92	18
regulation of small GTPase mediated signal transduction	GO:0051056	3.11E-02	42	11
histone lysine methylation	GO:0034968	3.42E-02	14	6
lipid transport	GO:0006869	3.70E-02	50	12
regulation of signaling	GO:0023051	3.94E-02	95	18
cellular response to stimulus	GO:0051716	4.30E-02	826	93
lipid localization	GO:0010876	4.66E-02	52	12

B.

aga-mir-2944a-5p				
Term Name	**ID**	**FDR**	**Term Size**	**Intersection Size**
Molecular Function				
protein binding	GO:0005515	3.46E-04	1791	150
purine ribonucleoside triphosphate binding	GO:0035639	6.99E-03	821	75
adenyl ribonucleotide binding	GO:0032559	6.99E-03	684	64
purine ribonucleotide binding	GO:0032555	6.99E-03	830	76
ribonucleotide binding	GO:0032553	6.99E-03	838	76
adenyl nucleotide binding	GO:0030554	6.99E-03	686	64
purine nucleotide binding	GO:0017076	6.99E-03	832	76
nucleoside phosphate binding	GO:1901265	6.99E-03	956	83
nucleotide binding	GO:0000166	6.99E-03	956	83
ATP binding	GO:0005524	6.99E-03	675	63
Rho guanyl-nucleotide exchange factor activity	GO:0005089	6.99E-03	27	8
kinase activity	GO:0016301	7.97E-03	290	33
Ras guanyl-nucleotide exchange factor activity	GO:0005088	7.97E-03	29	8
binding	GO:0005488	1.28E-02	4675	309
small molecule binding	GO:0036094	2.01E-02	1011	84
transferase activity, transferring phosphorus-containing groups	GO:0016772	2.07E-02	386	39
carbohydrate derivative binding	GO:0097367	2.17E-02	959	80
phosphotransferase activity, alcohol group as acceptor	GO:0016773	2.45E-02	264	29
Rho GTPase binding	GO:0017048	2.49E-02	36	8
phosphorus-oxygen lyase activity	GO:0016849	4.22E-02	23	6
drug binding	GO:0008144	4.60E-02	815	68
anion binding	GO:0043168	4.78E-02	979	79
Biological Process				
intracellular signal transduction	GO:0035556	4.13E-03	193	29

C.

aga-mir-309				
Term Name	**ID**	**FDR**	**Term Size**	**Intersection Size**
Molecular Function				
calcium ion binding	GO:0005509	1.91E-03	170	26

D.

as-mir16				
Term Name	**ID**	**FDR**	**Term Size**	**Intersection Size**
Molecular Function				
protein binding	GO:0005515	1.15E-02	1791	153
binding	GO:0005488	1.86E-02	4675	336

ID	Total Reads QC Passed	Mapping to Host Genome	Proportion of Total Mapping to Host	Mapping to Host miRNAs	Proportion of Host Reads Mapping to miRNAs	Mapping to Viral Genome	Proportion of Total mapping to Virus	Viral piRNAs	Proportion Mapping to Viral as Potential piRNAs
C_D2_R1	17800192	16126376	91%	3033086	19%	199006	1%	7960	4%
C_D2_R2	16812408	15056380	90%	2254482	15%	272599	2%	8569	3%
C_D2_R3	18092880	15127397	84%	2551279	17%	275676	2%	7103	3%
C_D7_R1	21189926	18142804	86%	179672	1%	797862	4%	16559	2%
C_D7_R2	14833688	13591924	92%	2254482	17%	96190	1%	6641	7%
C_D7_R3	20551719	18828285	92%	3617884	19%	187169	1%	8276	4%
C_D14_R1	20259396	18306112	90%	3576305	20%	180217	1%	10368	6%
C_D14_R2	17801450	16105271	90%	3033309	19%	140748	1%	8647	6%
C_D14_R3	18082055	16502692	91%	3794362	23%	148854	1%	10335	7%
V_D2_R1	15851816	14109550	89%	2798105	20%	214624	1%	9641	4%
V_D2_R2	18043897	15456543	86%	2600968	17%	317283	2%	13052	4%
V_D2_R3	17499685	14894859	85%	2076112	14%	255560	1%	10647	4%
V_D7_R1	15721343	14395463	92%	2977219	21%	262465	2%	11763	4%
V_D7_R2	23780788	21664761	91%	4000416	18%	277922	1%	17215	6%
V_D7_R3	20775885	18719374	90%	3376672	18%	295778	1%	16856	6%
V_D14_R1	18174128	16399105	90%	3227809	20%	332311	2%	16246	5%
V_D14_R2	19188815	17548223	91%	2658496	15%	303330	2%	12630	4%
V_D14_R3	20525522	18517727	90%	2897260	16%	309427	2%	16246	5%

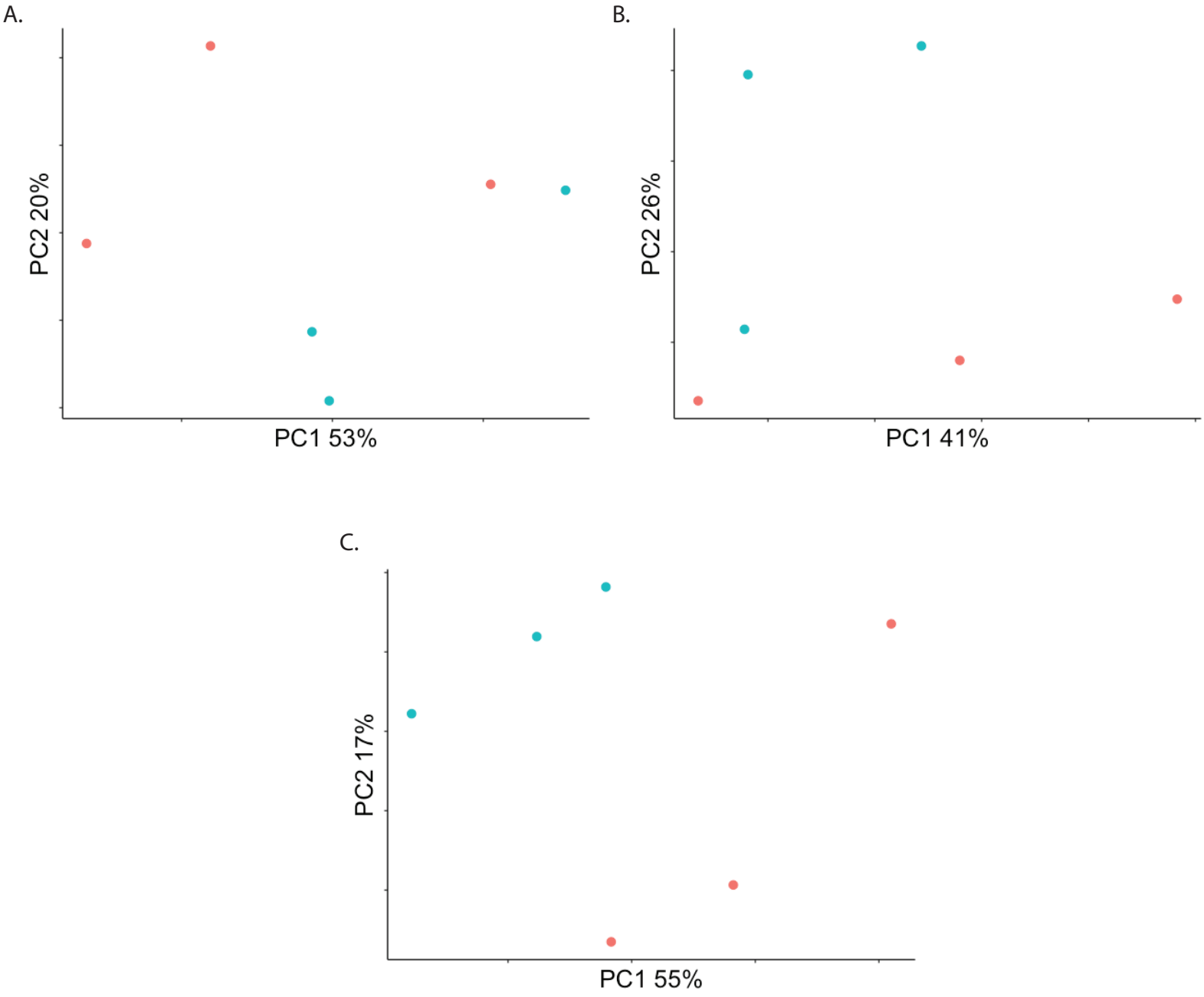

Figure 1: Principal Components Analysis (PCA) on filtered read counts mapping to annotated genes from the AsteI2 build of the *Anopheles stephensi* genome in Vectorbase. A., B., and C. are read counts from samples in the 2, 7, and 14 dpi groupings respectivey. In all PCAs, blue are Mayaro infected, and red are control.

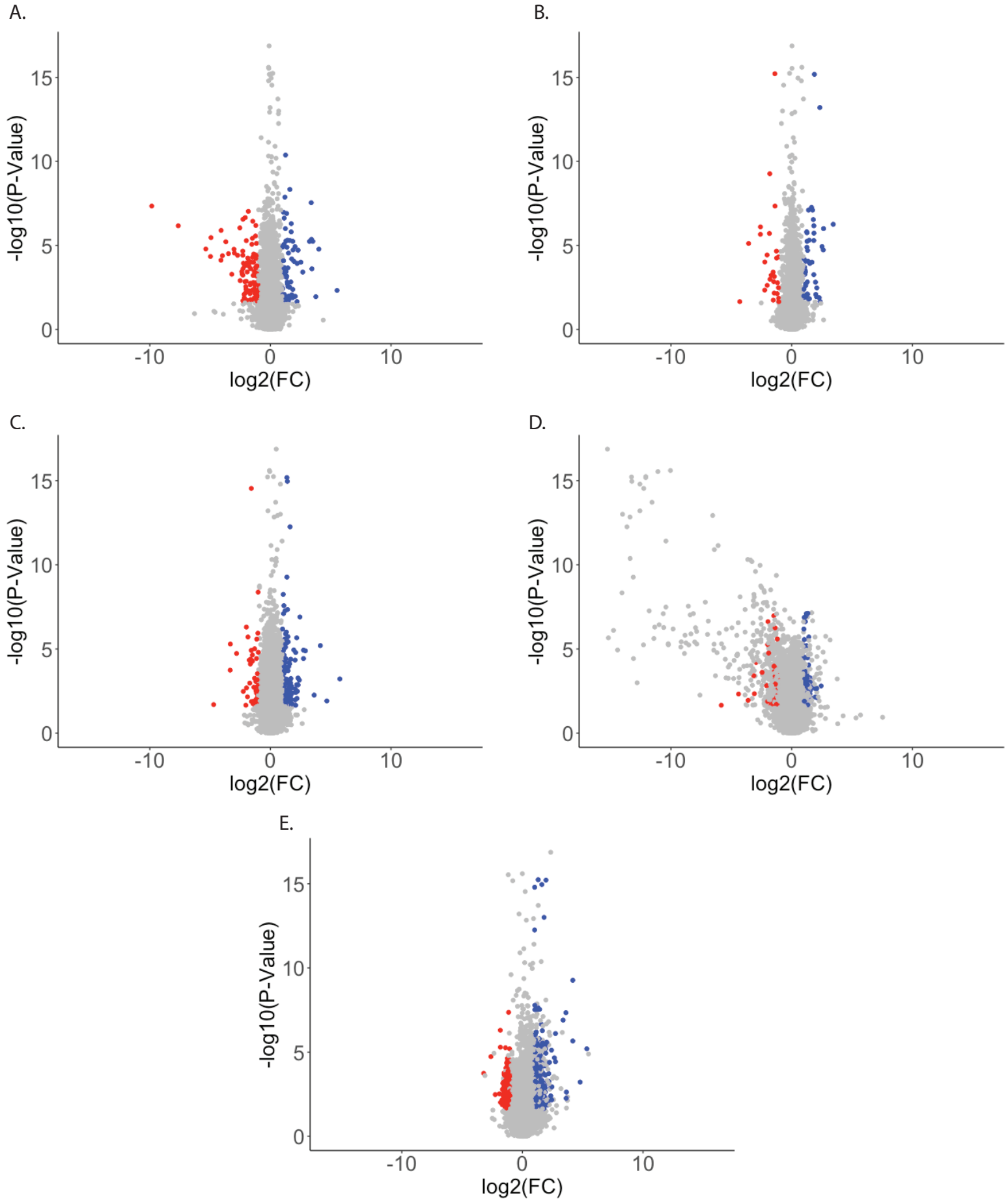

Figure 2: Volcano plots visualizing differential expression of Anopheles stephensi transcripts in response to Mayaro infection. The Y-axis shows -log10 transformed P-values, and the X-axis shows log2 transformed fold change values. Red points represent transcripts downregulated by more than -1 logFC in response to infection with a FDR < 0.05, while blue points are transcripts upregulated by more than 1 logFC in response to infection with a FDR < 0.05. A. - C. are trasncripts regulated in the 2 dpi, 7 dpi, and 14 dpi groupings respectively, while D. and E. are transcripts regulated in the infected treatment between 2 - 7 dpi and 7 - 14 dpi respectively.

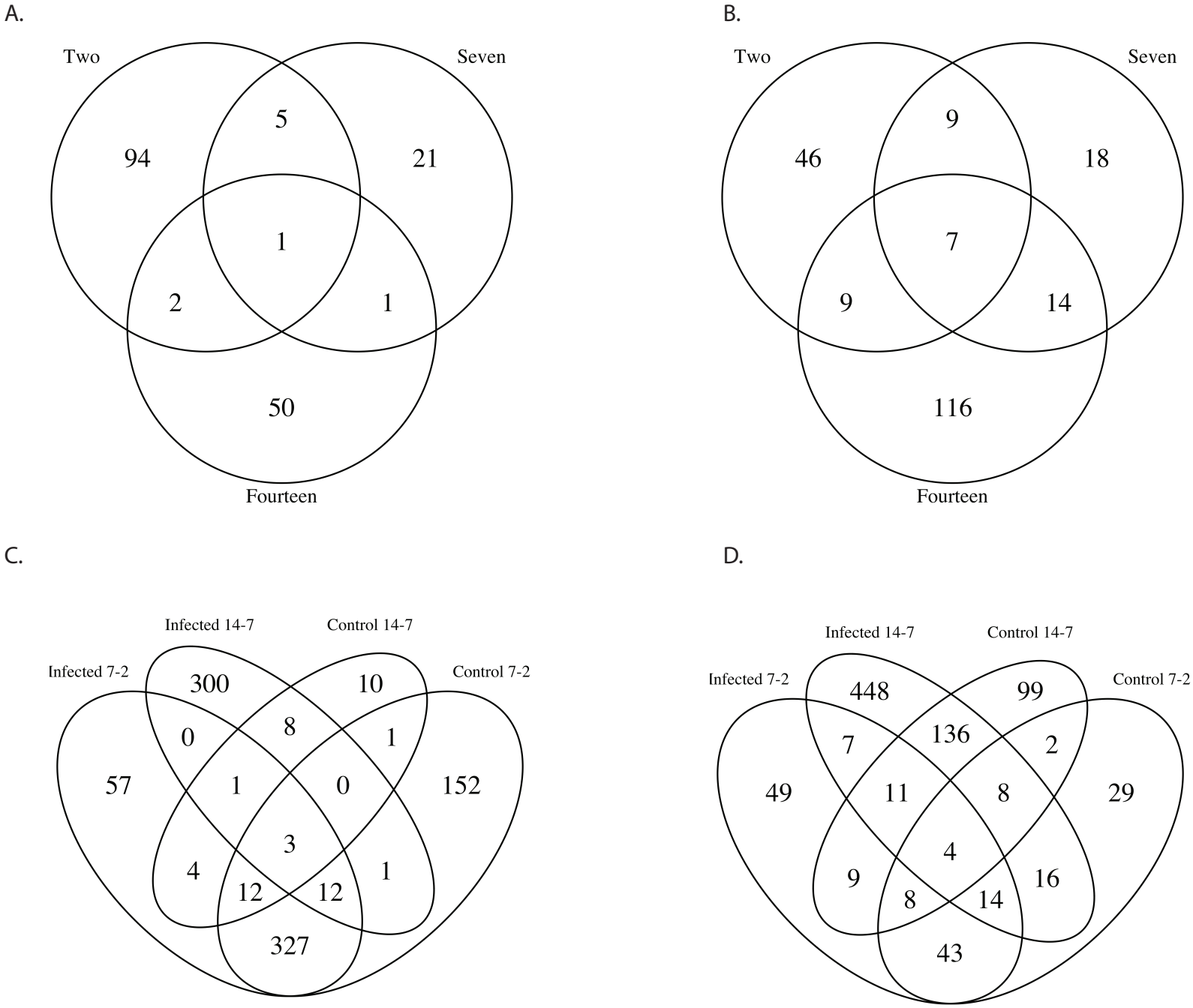

Figure 3: Venn diagrams demonstrating overlap of significantly regualted genes for different contrasts when running differential expression analysis using a negative binomial general lineriazed model. A. and B. demonstrate negatively and positively regulated genes respectively for 2, 7, and 14 dpi contrasts. C. and D. demonstrate negatively and positivey regulated genes respectively for 2-7 dpi and 7 - 14 dpi contrasts in the control and infected treatments.

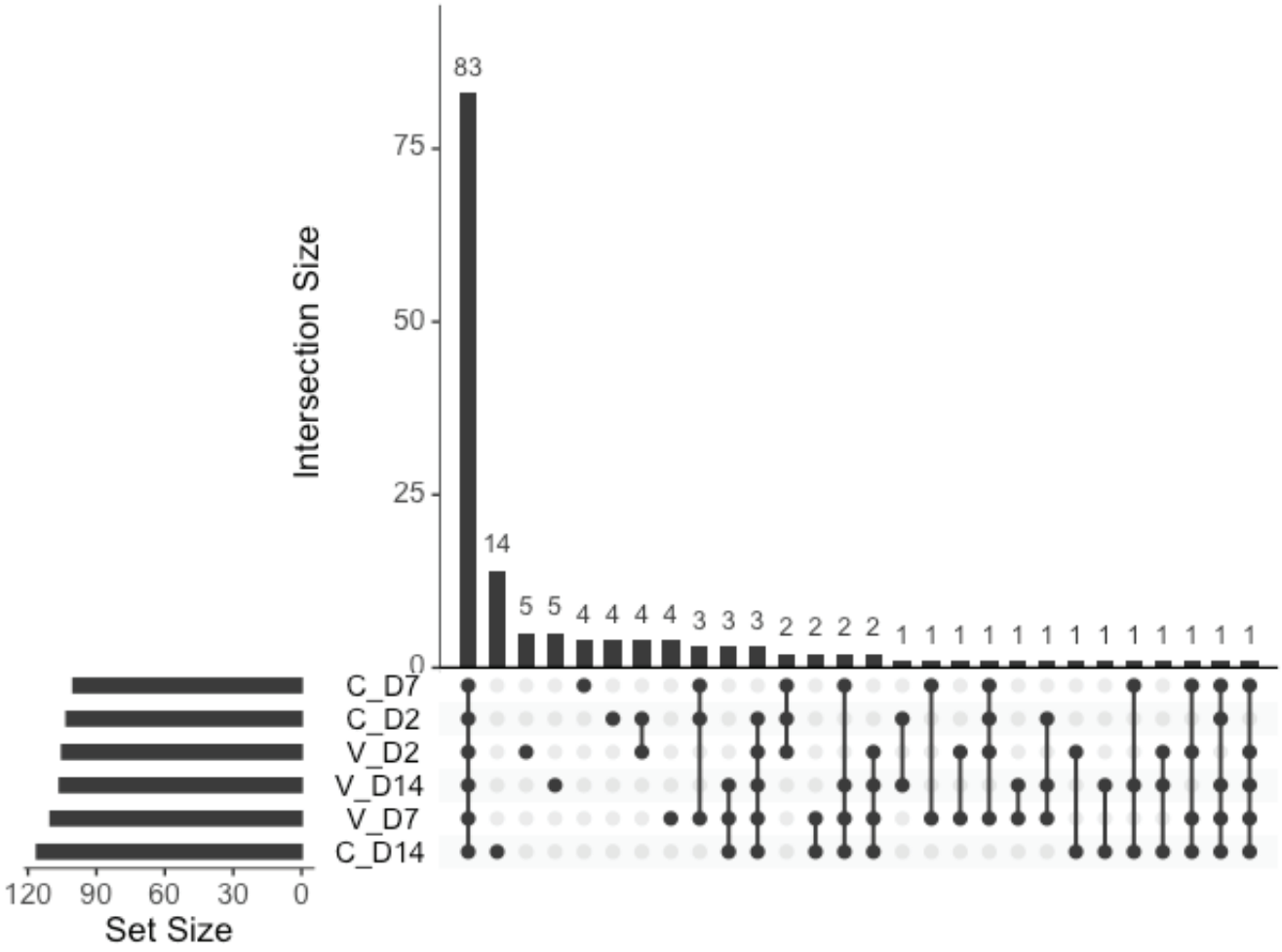

Figure 4: The top histogram represents the number of miRNAs shared between treatments (intersection size), and each row below the histogram represents a treatment. The lines connecting treatments below the top histogram represent treatments which share that number of miRNAs, and the histogram to the side of the treatments represents the number of miRNAs contained within each treatment.

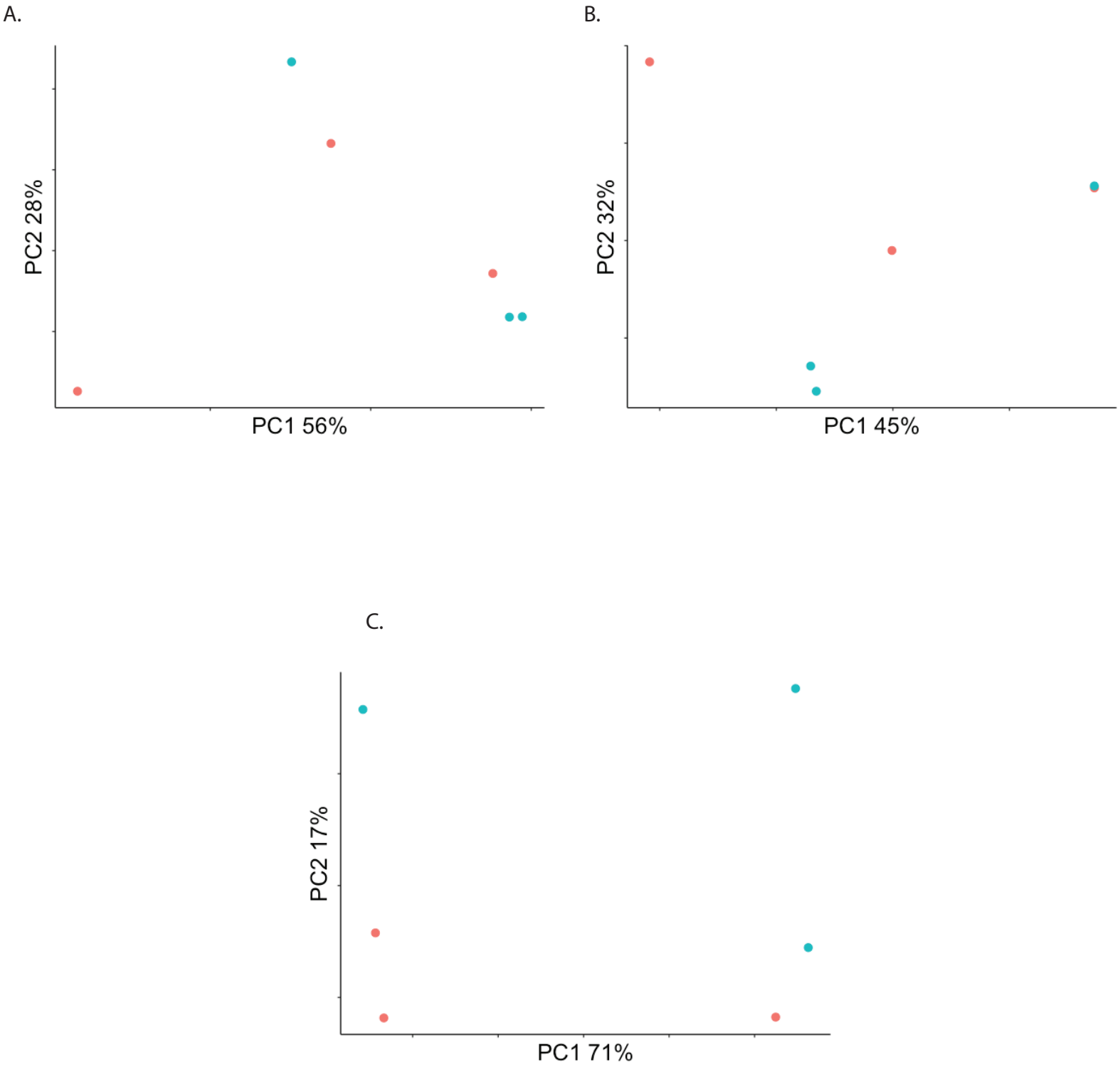

Figure 5: Principal Components Analysis (PCA) on read counts mapping to miRNAs identified in the AsteI2 build of the *Anopheles stephensi* genome in Vectorbase. A. - C. are the 2 dpi, 7 dpi, and 14 dpi groupings respectively. In all PCAs, blue is Mayaro infected, and red is control.

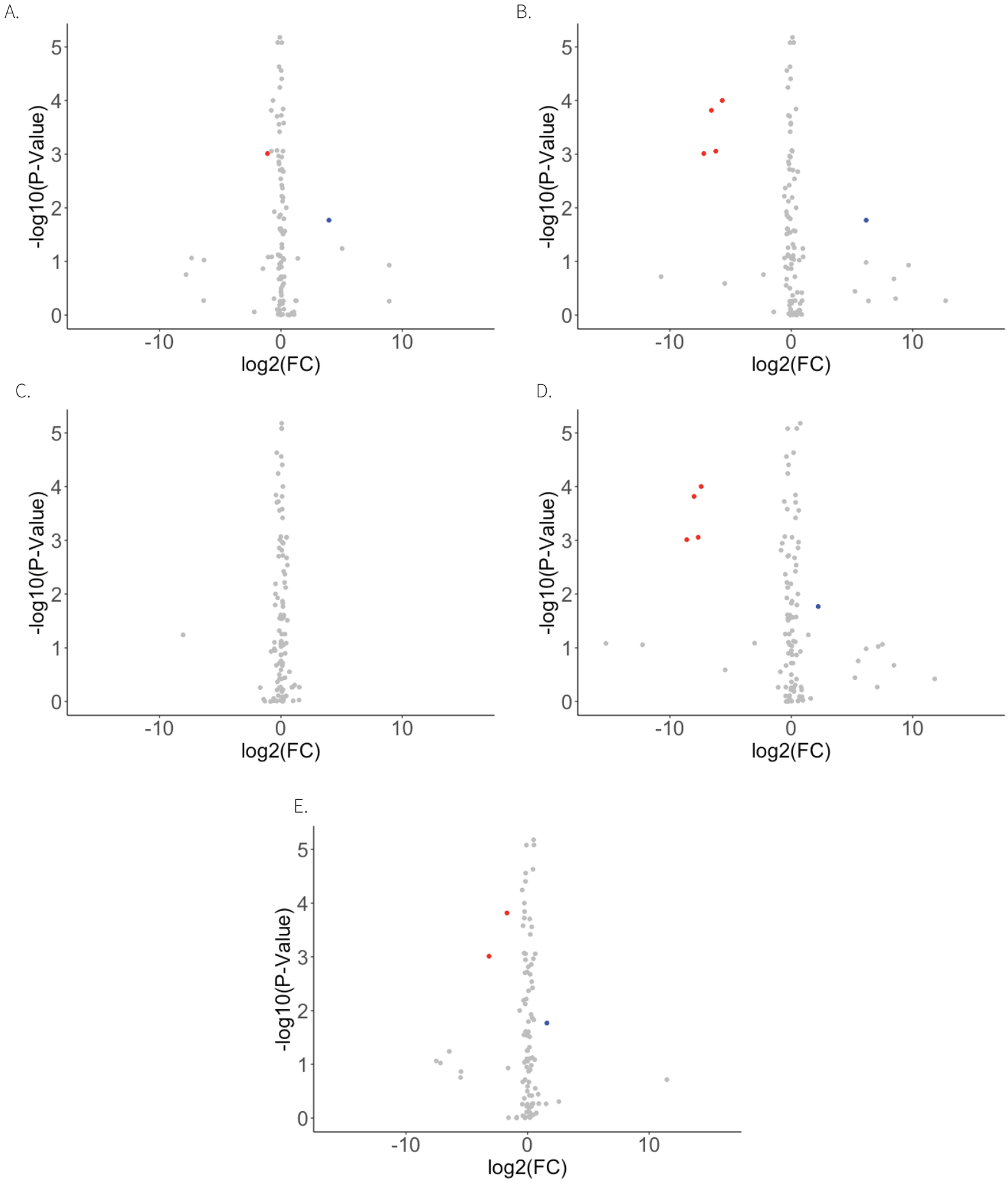

Figure 6: Volcano plots visualizing dierential expression of identified *Anopheles stephensi* miRNAs in response to Mayaro infection. The Y-axis shows -log10 transformed P-values, and the X-axis shows log2 transformed fold change values. Red points represent transcripts downregulated by more than -1 logFC in response to infection with a FDR < 0.05, while blue points are transcripts upregulated by more than 1 logFC in response to infection with a FDR < 0.05.
A. - C. are the 2 dpi, 7 dpi, and 14 dpi groupings respectively, while D. and E. are miRNAs regulated in the infected treatment between 2 - 7 dpi and 7 - 14 dpi respectively.

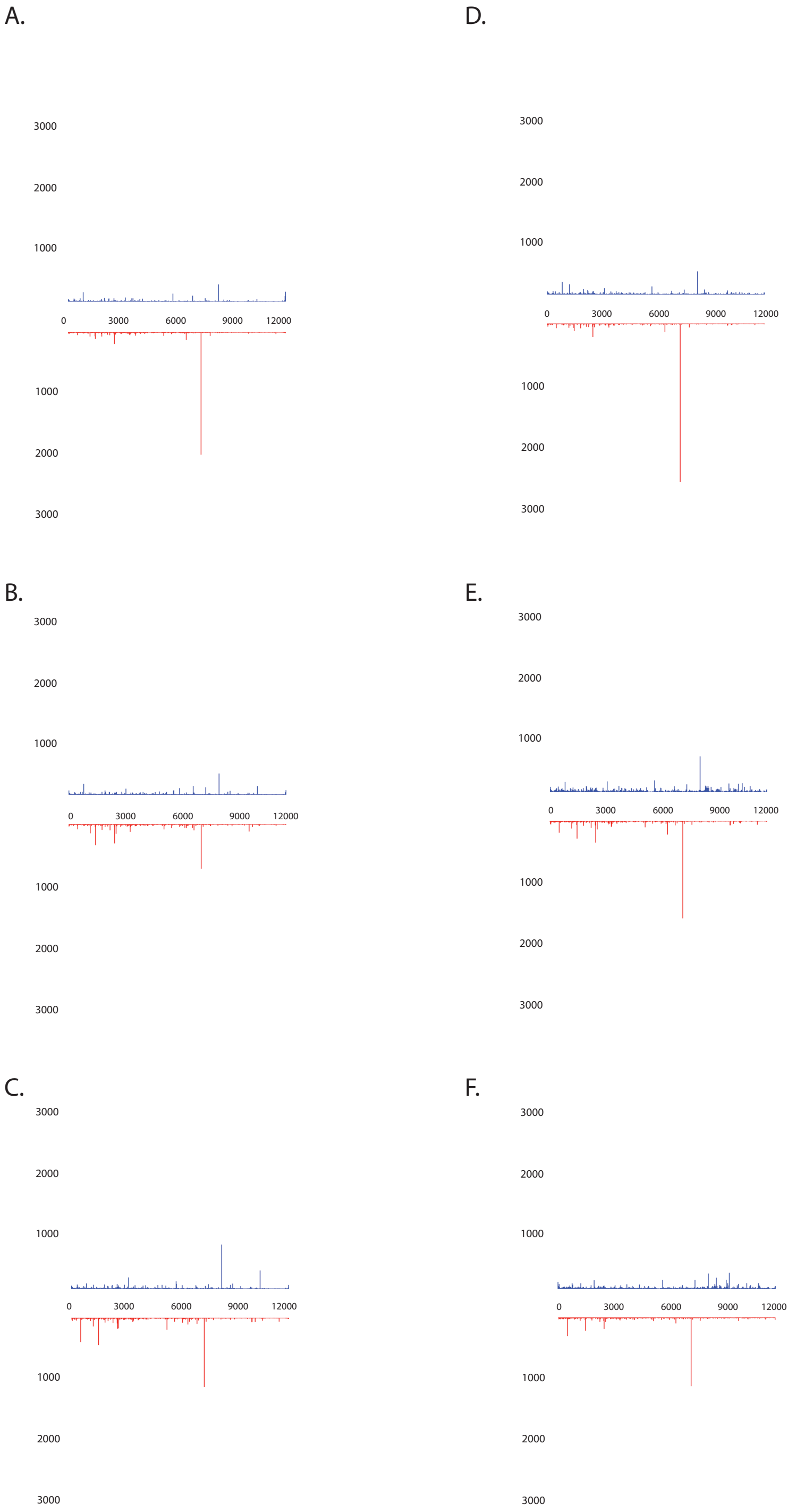

Figure 7: Histograms demonstrating read depth across the Mayaro virus genome for reads with a piRNA size profile (24 - 30 nt). Y-axis is red depth, and X-axis is position in viral genome. Blue demonstrates reads for that sample mapping to the positive strand, while red demonstrates those mapping to the negative strand. A. - C. are control for 2, 7, and 14 dpi respectively, and D. - F. are infected for 2, 7, and 14 dpi. One replicate per treatment is chosen here to demonstrate, but all replicates are in Suplementary Figure 1.

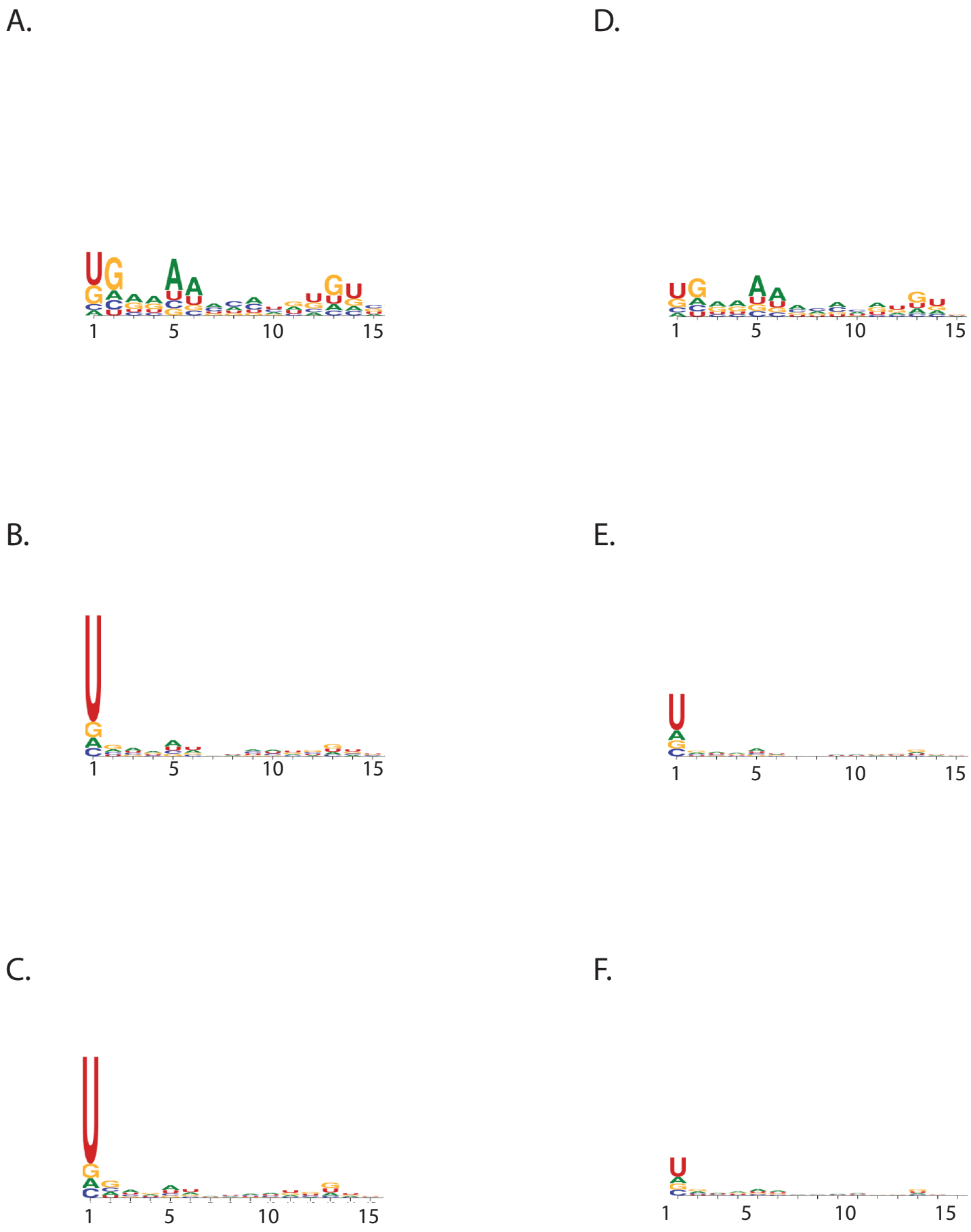

Figure 8: Nucleotide bias at first 15 bp of potential piRNA reads mapping to the Mayaro virus genome. X-axis is position in read, and Y-axis is nucleotide bias. Size of nucleotide demonstrates relative bias at that position in the read. A. - C. are control for 2, 7, and 14 dpi respectively, and D. - F. are infected for 2, 7, and 14 dpi. One replicate per treatment is chosen here to demonstrate, but all replicates are in Suplementary Figure 2.